Deterministic and stochastic parameterizations of kinetic energy backscatter in the NEMO ocean model in Double-Gyre configuration

To cite this article: P Perezhogin 2019 *IOP Conf. Ser.: Earth Environ. Sci.* **386** 012025

Deterministic and stochastic parameterizations of kinetic energy backscatter in the NEMO ocean model in Double-Gyre configuration

P Perezhogin
Marchuk Institute of Numerical Mathematics of the Russian Academy of Sciences, Moscow, Russia
E-mail: pperezhogin@gmail.com

Abstract. Eddy-permitting numerical ocean models often resolve mesoscale turbulence only partly, which leads to underestimation of eddy kinetic energy (EKE). Mesoscale dynamics can be amplified by using kinetic energy backscatter (KEB) parameterizations returning energy from the unresolved scales. We consider two types of KEB: stochastic and negative viscosity ones. The tuning of their amplitudes is based on a local budget of kinetic energy, thus, they are "energetically-consistent" KEBs. In this work, KEB parameterizations are applied to the NEMO ocean model in Double-Gyre configuration with an eddy-permitting resolution (1/4 degree). To evaluate the results, we compare this model with an eddy-resolving one (1/9 degree). We show that with the KEBs the meridional overturning circulation (MOC), meridional heat flux, and sea surface temperature (SST) can be significantly improved. In addition, a better match has been found between the time power spectra of the eddy-permitting and the eddy-resolving model solutions.

1. Introduction

Numerical ocean models used in climate research [1] have a relatively coarse resolution to properly resolve mesoscale eddies, which contribute largely to the transport of tracers and momentum. Mesoscale eddies emerge on the length scale of the Rossby radius of deformation due to baroclinic instability, and in the midlatitude ocean their qualitative length scale is 30 km. Considering the ability to resolve mesoscale eddies, the ocean general circulation models (OGCMs) can be divided into three groups: "non-eddy-resolving" models have an approximate resolution of 1^o and cannot simulate the generation of mesoscale eddies; "eddy-resolving" models have several mesh points for a mesoscale eddy and their resolution is 10 times finer. Finally, there are models named "eddy-permitting" which have an intermediate resolution. In the eddy-permitting models eddies are represented in a computational grid, but their dynamics and generation are damped. Currently the OGCMs in climate models are moving from non-eddy-resolving to eddy-permitting resolutions.

In the non-eddy-resolving models there are two main parameterizations of subgrid eddies (i.e. unrepresented in the grid): usual turbulent diffusion/viscosity and Gent-McWilliams (GM) diffusion of layer thickness [2]. The former models turbulent mixing of resolved fields by subgrid eddies, while the latter reduces the slope of isopycnals, thereby introducing a sink of available potential energy (APE) required to mimic baroclinic instability occurring on unresolved scales. Turbulent diffusion at non-eddy-resolving resolutions is usually designed with a Laplace operator acting along isopycnal surfaces

[3]. Subgrid parameterizations at eddy-permitting resolution are substantially different. Diffusion and viscosity operators are usually changed to a squared Laplace (biharmonic) one acting along the horizontal direction. Thus, its purpose is not to perform mixing, but to ensure stability of the simulation to reduce damping of mesoscale eddies. Also, the GM parameterization is not recommended for the eddy-permitting models [4].

Kinetic energy backscatter (KEB) is a parameterization which returns energy from unresolved turbulent scales to resolved ones, contrary to eddy viscosity. This parameterization models poorly resolved inverse energy cascade inherent to 2D turbulence [5]. The first turbulence closures of this type were tested in a simple barotropic model [6] and later in an atmosphere ensemble prediction system [7]. Recently it was proposed to use KEB parameterizations to improve eddy-permitting ocean simulations [8], [9]. The simplest KEB closures are based on the Laplace operator with a negative viscosity coefficient [8], [9] or on a stochastic tendency [8], [10]. Both types of the KEB were shown to be effective in restoration of the barotropic eddy kinetic energy spectrum [8], [9], [11], and they can improve the mean flow [8], [9]. In spite of the success of these parameterizations in simulations with simplified quasi-geostrophic equations, we can mention only one paper where the KEB was applied to a primitive-equation ocean model [12].

In this work we apply two KEB parameterizations, negative viscosity and stochastic ones, to improve the NEMO ocean model [3] at coarse eddy-permitting resolution ($1/4^o$) in Double-Gyre configuration [13]. Intending to improve the mesoscale physics, we compare coarse models with respect to an eddy-resolving one ($1/9^o$), which allows for mesoscales eddies, but not submesoscale ones. Both KEBs are "energetically consistent", which means that we tune the KEB amplitude to compensate the energy loss due to eddy viscosity. Similarly to [9] and [12], we define the negative viscosity KEB as a Laplace operator with a negative viscosity coefficient depending on the amount of subgrid energy. The computation stability is ensured by biharmonic eddy viscosity damping. The stochastic KEB has the functional form of a random streamfunction weighted by the local dissipation rate, as proposed in [7]. The spatial correlation is controlled by multiple applications of a simple spatial filter to the generated spatial white noise, as proposed in [10]. Both KEB parameterizations increase the eddy kinetic energy (EKE) in an eddy-permitting model. It makes the meridional eddy heat flux close in eddy-permitting and eddy-resolving models. As a result, the sea surface temperature (SST) and the meridional overturning circulation (MOC) were restored with the use of KEB. Finally, we report improvements in the time power density spectrum.

2. Double Gyre setting

We use an open access NEMO model (version 3.6) [14] in Double-Gyre configuration described in [13]. Note that there is some discrepancy in the parameters between the open access Double Gyre code and paper [13]. We hope that this is the reason why we have some quantitative differences. If it is not mentioned, we do not change the source code. The ocean model solves primitive equations (the vectors are in bold):

$$\frac{dT}{dt} = F_T, \frac{dS}{dt} = F_S, \quad (1)$$

$$\frac{\partial \boldsymbol{U}_h}{\partial t} + adv_h + cor_h = -\frac{1}{\rho_0}\nabla_h p + \boldsymbol{F}_{\boldsymbol{U}_h}, \quad (2)$$

$$\frac{\partial \eta}{\partial t} = -H\nabla_h \bar{\boldsymbol{U}}_h, \quad (3)$$

$$\frac{\partial p}{\partial z} = -\rho g, \nabla \cdot \boldsymbol{U} = 0, \quad (4)$$

$$\rho = \rho_0\big(1 - a(T - T_0) + b(S - S_0)\big), \quad (5)$$

where $T, S, \boldsymbol{U}, \eta, \rho, p$ are the potential temperature, salinity, velocity, free surface height, density, and pressure; $\boldsymbol{U}_h$ is the horizontal part of the velocity, and $\bar{\boldsymbol{U}}_h$ is its vertical average. $F_T, F_S, \boldsymbol{F}_{\boldsymbol{U}_h}$ are the external forcings and physical parameterizations. We introduce a Lagrangian derivative $\frac{d}{dt} = \frac{\partial}{\partial t} +$

$(\boldsymbol{U}\cdot\nabla)$, a nabla operator $\nabla=(\partial_x,\partial_y,\partial_z)$, and its horizontal part $\nabla_h=(\partial_x,\partial_y)$. Exact expressions for the advective and Coriolis terms adv_h and cor_h are given in [14]. In our configuration the free surface equation (3) and the equation of state (EOS (5)) are linear. The EOS parameters are as follows: $\rho_0=1026\,kg\,m^{-3}$, $a=2\cdot10^{-4}K^{-1}$, $b=7.7\cdot10^{-4}psu^{-1}$, $T_0=10C^o$, $S_0=35psu$. The computational domain is a flat-bottomed rectangular box $L_x\times L_y\times L_z=3180\,km\times2120\,km\times4\,km$ in the β-plane approximation with free-slip and no heat flux, no salt flux spatial boundary conditions, and quadratic bottom drag. The basin is centered at $\sim30^oN$ and rotated by 45^o to the zonal direction, in lat-lon coordinates; it is shown in Figure 1. Note that the metric terms inherent to spherical geometry are excluded.

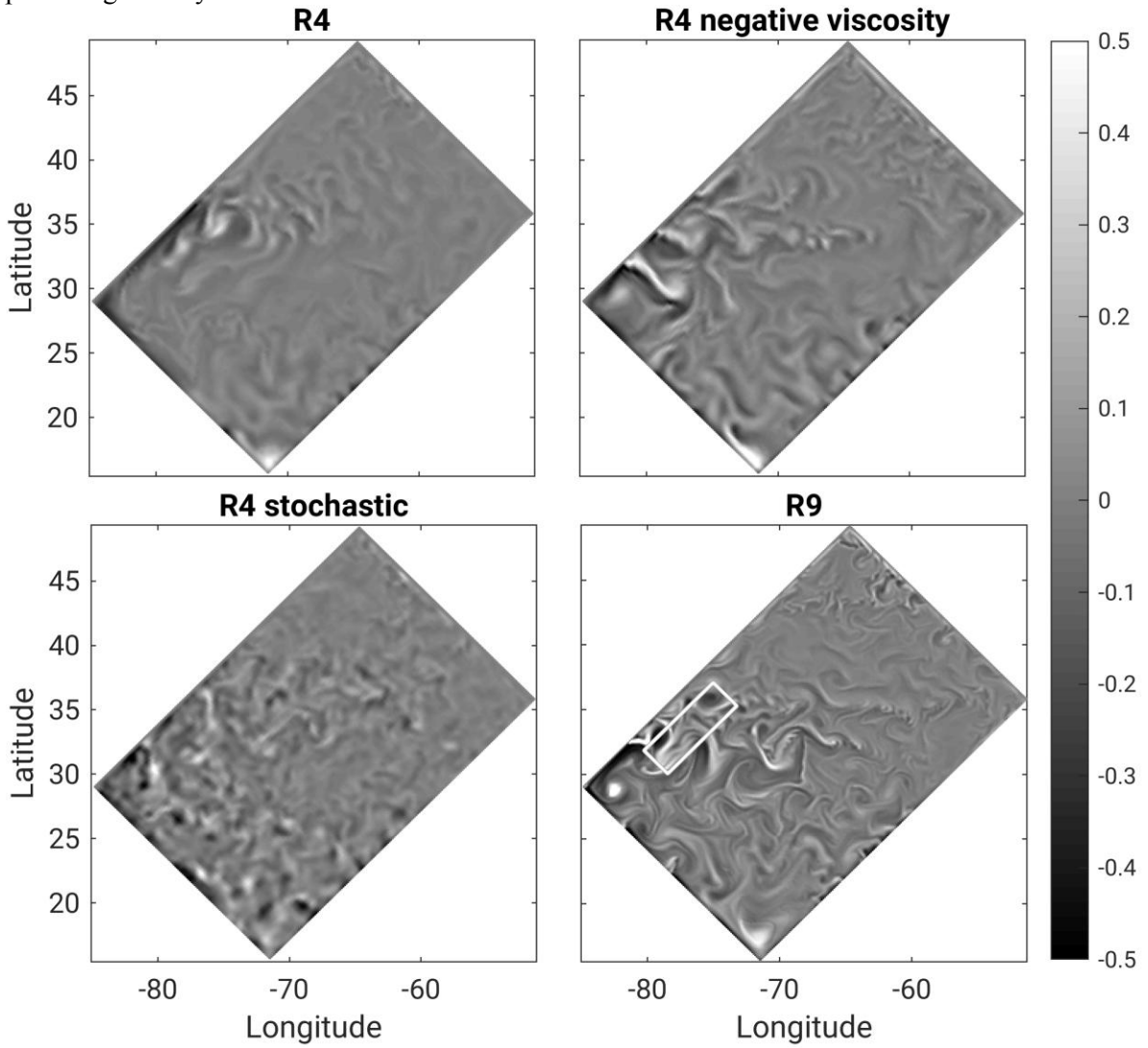

Figure 1. Snapshot of surface relative vorticity in f (Coriolis parameter) units. 30 March after spin-up. R4 – eddy-permitting model, R9 – eddy-resolving model, R4 negative viscosity and R4 stochastic – eddy-permitting models with KEB parameterizations. Colorbar is saturated at ±0.5. The white rectangle is explained in Figure 4.

The free surface is stressed by zonal wind having its maximum eastward speed at 36^oN and maximum westward speed at 22^oN . The following three surface buoyancy fluxes sustain a south-north decline of the surface temperature and the growth of surface salinity. The conductive heat flux from the atmosphere is given by $Q=\gamma(T_{atm}-SST)$, SST and T_{atm} – the surface ocean temperature and the

atmosphere temperature, $\gamma = 40 W m^{-2} K^{-1}$. Also, solar radiation and fresh water fluxes are prescribed at the surface. The listed forcings vary with latitude and seasonally and are given in [13].
We consider models with three uniform spatial resolutions. The parameters are given in Table 1. R1 is initialized at rest with vertical profiles of temperature and salinity uniformly applied to the whole basin [13]. The number of vertical layers is 30 for all simulations. We accomplish spin-up of R4 and R9 models, first running R1 model for 1000 years and then continuing the computations with R4 or R9 models for 120 years. The last 20 years are stored for analysis. The Rossby deformation radius for the resulting stratification varies from 40 km in the south to 5 km in the north [13]. The diffusion/viscosity coefficients for models R1 and R9 are taken from [13]. The viscosity in model R4 is almost the smallest possible. Further decreasing leads to wrong reproduction of the meridional eddy heat flux.

Table 1. Model experiments (R1, R4, R9) and their parameters. Unless otherwise mentioned, diffusivity/viscosity act in horizontal direction.

	R1, non-eddy-resolving	R4, eddy-permitting	R9, eddy-resolving
$n_X \times n_y \times n_z$	$30 \times 20 \times 30$	$120 \times 80 \times 30$	$270 \times 180 \times 30$
mesh step	$1^o, 106\ km$	$1/4^o, 26.5\ km$	$1/9^o, 11.7\ km$
time step	120 min	30 min	800 sec
eddy diffusivity	Isoneutral ∇_h^2, $10^3 m^2 s^{-1}$	$\nabla_h^4,\ -10^{10} m^4 s^{-1}$	$\nabla_h^4,\ -10^9 m^4 s^{-1}$
eddy viscosity	$\nabla_h^2,\ 10^5 m^2 s^{-1}$	$\nabla_h^4,\ -5 \cdot 10^{11} m^4 s^{-1}$	$\nabla_h^4,\ -5 \cdot 10^{10} m^4 s^{-1}$

3. Kinetic energy backscatter (KEB) parameterizations

3.1. Negative viscosity KEB

This parameterization supplements horizontal biharmonic momentum damping in the momentum equation with (2) additional term returning the energy in the form of a Laplace operator, as proposed in [8]:

$$\frac{\partial \boldsymbol{U}_h}{\partial t} = \cdots \nu_4 \nabla_h^4 \boldsymbol{U}_h + \nabla_h (\nu_2 \nabla_h \boldsymbol{U}_h). \qquad (6)$$

Here ∇_h is assumed to act on the vector componentwise. When $\nu_4 < 0$, the grid-scale numerical noise is effectively dissipated. The viscosity $\nu_2 \leq 0$ must be negative to return the energy. The choice of a Laplace operator for KEB is natural, since it is the simplest linear operator with a characteristic length scale larger than that of the biharmonic operator. Moreover, it is shown by R. Kraichnan in [15] that subgrid 2D turbulence produces a tendency represented by the Laplace operator in the middle and large scales with a negative viscosity coefficient. To take into consideration spatial non-homogeneity of the eddy field and weak dynamics near the bottom, we follow works [9], [16], and [12] and introduce dependence on the coordinates $\nu_2(x, y, z, t) \leq 0$. ν_2 is found based on the "energetically consistent" property: the joint energy flux to subgrid scales corresponding to the Laplace and biharmonic operators must be zero. This property is consistent with the idea of inverse energy cascade: the energy shall not pass to subgrid scales. The energy fluxes to subgrid scales related to the biharmonic and Laplace operators are expressed in Galilean invariant form following [16]:

$$\dot{E}_{diss} = \nu_4 \nabla_h \boldsymbol{U}_h \cdot \nabla_h \left(\nabla_h^2 \boldsymbol{U}_h \right), \qquad (7)$$

$$\dot{E}_{back} = \nu_2 \nabla_h \boldsymbol{U}_h \cdot \nabla_h \boldsymbol{U}_h. \qquad (8)$$

The signs of the fluxes are as follows: $\int \dot{E}_{diss}\, dxdydz > 0, \int \dot{E}_{back}\, dxdydz \leq 0$. Local equalization of these fluxes $\dot{E}_{diss}(x, y, z, t) + \dot{E}_{back}(x, y, z, t) = 0$ leads to an ill-posed problem for finding ν_2 if

$|\nabla_h \boldsymbol{U}_h| = 0$. To overcome it, papers [9] and [16] introduced an equation for subgrid energy ($e \equiv e(x,y,z,t)$), which is produced by dissipation ($\dot{E}_{diss}$) and lost to the resolved scales ($\dot{E}_{back}$):

$$\frac{de}{dt} = c_{diss}\dot{E}_{diss} + \dot{E}_{back} + \nu_e \nabla_h^2 e. \qquad (9)$$

Here d/dt is the Lagrangian derivative (advection), which is implemented in the code with the simplest upwind scheme [14], $\nu_e = 1000 m^2 s^{-1}$ is equal to the diffusivity of eddies in model R1. Contrary to [16], we apply the Lagrangian derivative instead of a partial derivative, which seems to be more physical and was originally proposed for the subgrid energy equation in [17]. As in [12], $c_{diss} \in (0,1)$ allows one to reduce the backscatter power. We found $c_{diss} = 0.8$ to be satisfactory. Larger values produce overestimated strong vortices and a strong meridional eddy heat flux near the surface at the WBC separation latitude. The subgrid energy e defines the negative viscosity:

$$\nu_2 = -c_{back}\Delta x\sqrt{\max(e,0)}, \qquad (10)$$

where Δx is the grid spacing and $c_{back} = 0.4\sqrt{2}$, as in [9]. The max-function allows us to treat situations when subgrid energy is negative, which can occur since the biharmonic operator is not positive definite. For the terms $\nabla_h(\nu_2 \nabla_h \boldsymbol{U}_h)$ in (6) and $\nu_e \nabla_h^2 e$ in (9), Neumann boundary conditions are applied: $(\nabla_h \boldsymbol{U}_h)\cdot \boldsymbol{n} = 0$ and $(\nabla_h e)\cdot \boldsymbol{n} = 0$, $\boldsymbol{n}$ is the normal vector to the horizontal boundary. As in [9], we report weak sensitivity of the results on the model for the e used. Our understanding is that an additional equation for subgrid energy is needed only to make the problem for finding ν_2 well-posed. In the next section it will be shown that the stochastic KEB can be tuned without an additional equation for subgrid energy.

3.2. Stochastic KEB

Let us construct a quasi-barotropic (quasi-2D) stochastic streamfunction as proposed in [7]:

$$\psi(x,y,z,t^n) = \phi(x,y,t^n)\cdot A(x,y,z,t^n), \qquad (11)$$

where $\phi(x,y,t^n)$ is a discrete random field. ϕ is independent at each mesh point and time layer t^n (i.e. discrete-space-time white noise) and has distribution $N(0,1)$ with zeros at the boundary. A is the amplitude controlling the energy input. The streamfunction modifies the momentum equation (2) as follows:

$$\frac{\partial \boldsymbol{U}_h}{\partial t} = \cdots + \alpha \nabla_h^{\perp} S^n(\psi), \qquad (12)$$

where $\nabla_h^{\perp} = (-\partial_y, \partial_x)$. α will be defined later. The function $S^n(\cdot)$ introduces n applications of a spatial discrete filter:

$$S(\psi) = \psi + \frac{(\Delta x)^2}{8}\nabla_h^2 \psi. \qquad (13)$$

This filter is based on the Laplace operator already contained in the model and nullifies the checkerboard grid noise ($(-1)^{i+j}$; i and j are indexes along the $x-$ and $y-$ directions) if a second order approximation is used. Zero Dirichlet boundary conditions are applied. The physical reasoning for stochastic parameterization with spatial white noise is again taken from [15], where subgrid turbulence was shown to produce stochastic forcing in small resolved scales. In contrast to [10], we generate random streamfunction, instead of random Reynolds stress components. Streamfunction approach gives analogous wavenumber spectrum, but doesn't require removing divergence of the resulting forces in momentum equation [18]. According to [10], the filter $S^n(\cdot)$ can be considered as a correction of a sharp wavenumber spectrum near the grid scale to account for numerical effects of non-spectral advection schemes. Also, the filter defines the correlation radius of the resulting parameterization. We use $n = 6$, which gives a correlation radius of several mesh points.

Contrary to the negative viscosity KEB, local equalization of the energy fluxes $\dot{E}_{diss}$ and $\dot{E}_{back}$ is possible without an additional equation for subgrid energy. According to [19], energy generation by the white noise process is proportional to the squared amplitude ($\dot{E}_{back} \sim -A^2$) and, hence, we choose:

$$A(x,y,z,t^n) = \sqrt{\max\left(\dot{E}_{diss},0\right)}. \qquad (14)$$

Finally, the energy generation and dissipation fluxes integrated over the domain should be equal. Again, using [19] we compute the energy generation for white noise and obtain a relation for finding α:

$$\frac{\alpha^2\Delta t}{2}\int\left\langle\left|\nabla_h^{\perp}S^n(\psi)\right|^2\right\rangle dxdydz = \int \dot{E}_{diss}dxdydz. \qquad (15)$$

Here Δt is the time step, and the angle brackets $\langle\cdot\rangle$ denote averaging over realizations of the random field ϕ. The left-hand side of the above equation can be estimated analytically taking into consideration knowledge of the wavenumber spectra [7], but still with simplifications. Our novelty is to drop averaging over an ensemble:

$$\int\left\langle\left|\nabla_h^{\perp}S^n(\psi)\right|^2\right\rangle dxdydz \approx \int\left|\nabla_h^{\perp}S^n(\psi)\right|^2 dxdydz, \qquad (16)$$

where the right-hand side is computed directly for the current realization of φ. This method is based on the following facts: 1) the ensemble-mean of RHS equals LHS 2) the standard deviation of RHS is 7% of its mean value.

4. Results

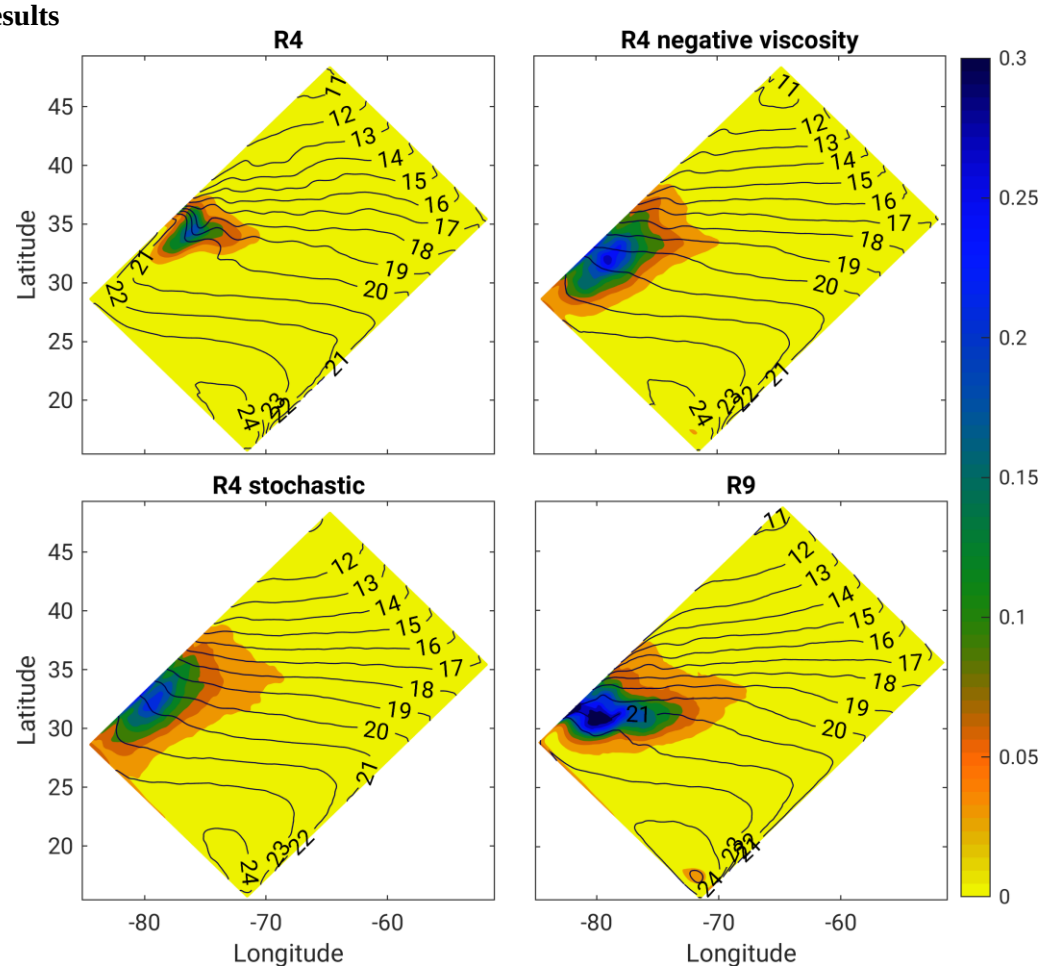

Figure 2. In colour: 20-year mean surface eddy kinetic energy (EKE), m^2/s^2. The colorbar is saturated at 0.3. In contours: 20-year mean sea surface temperature (SST), C^o. R4 – eddy-permitting model, R9 – eddy-resolving model, R4 negative viscosity and R4 stochastic – eddy-permitting models with KEB parameterizations.

We consider 4 models: an eddy-permitting model R4, an eddy-resolving model R9, and R4 with two KEB parameterizations: negative viscosity and stochastic ones. They are spun up as described in Section 2. Unless otherwise mentioned, we show the results averaged over the last 20 years. The model in Double Gyre setting simulates the western boundary current (WBC) similar to Gulfstream or Kuroshio. At some latitude, the WBC separates from the boundary forming, in the zonal direction, an offshore extension which divides the north and south gyres (see Figure 1). The separation latitude is strongly dependent on the resolution, and it moves to the south as the mesoscale and submesoscale eddies become resolved [13]. The WBC separation point and its extension strength are strongly associated with the sea surface temperature (SST) and the sea surface height (SSH), since their isolines pass along the jet current. Figure 2 shows the 20-year mean SST in contours for 4 models. The major discrepancy between models R4 and R9 is in isotherms 21 and 22. Applying the KEB straightens these isotherms, which leads to a significant fall of the errors in the mean surface fields (see Table 2). Improvements in the mean fields results from the amplification of the eddy activity, whose strength can be attributed to the eddy kinetic energy (EKE) level. Applying the KEB parameterizations allows us to increase the surface-averaged EKE (see Table 2) and – concerning its spatial distribution – to shift its maximum southward (see Figure 2 in colour). However, we point out that the surface EKE in models R4 with KEBs is elongated along the boundary, contrary to elongation in the zonal direction in model R9. It means that long jet extension cannot be simulated at a coarse grid even with KEB parameterizations.

Table 2. 20-year mean surface-averaged EKE and norm of errors in SST (sea surface temperature) and SSH (sea surface height) fields in models R4 with respect to reference R9. Two norms for any $\varphi(x,y)$ are $(|\varphi_{R4} - \varphi_{R9}|)$and $mean(|\varphi_{R4} - \varphi_{R9}|)$.

	R4	R4 negative visc.	R4 stochastic	R9
surf. EKE, $m^2 s^{-2}$	0.01	0.023	0.027	0.025
error SST, C^o	7.0; 0.40	3.1; 0.30	4.3; 0.27	
error SSH, m	0.68; 0.062	0.38; 0.039	0.40; 0.040	

One of the most apparent indicators of the eddy activity is the transport of tracers. Under the prescribed surface heat fluxes, ocean flows produce meridional heat transport (MHT) towards north: $Q = \rho_0 C_p TV$, $C_p \approx 3992 JK^{-1}kg^{-1}$ is the heat capacity, and V is the meridional velocity. Note that we neglect the heat transport corresponding to diffusion, since its action is minimized with the use of a biharmonic operator. The MHT consists of two parts: mean-flow meridional heat transport (MMHT, $\rho_0 C_p \bar{T}\bar{V}$, the overline stands for time-averaging over the last 20 years) and eddy meridional heat transport (EMHT). The EMHT strongly depends on the resolution, and it is almost zero for model R1. Models R4 and R9 have a significant EMHT: of the order of the MMHT (see [13] for details). The distribution of the EMHT in depth for models R4 and R9 is shown in Figure 3 by colour. In model R9, the most significant EMHT (note the logarithmic depth-scale) corresponds to a region $200m - 500m$ in depth and $23^oN - 30^oN$. The heat in this region fluxes southward, which is consistent with the northward gradient of potential temperature at this depth (not shown). Both KEB parameterizations amplify this flux in model R4 and break the wrong negative heat flux in the region of $32^oN - 35^oN$.

The meridional overturning circulation (MOC) is shown by contours in Figure 3. The MOC is described by the following streamfunction: $\Psi_{MOC}(y',z) = \int_{-H}^{-z} \bar{V}(x',y',z',t)dx'dz'$, where x' and y' are the coordinates along longitude and latitude, $z \in (-H, 0)$ is the depth, the overline is time averaging over 20 years, and V is the meridional velocity. The circulation in all models consists of 4 cells, and the largest one is at the bottom (note logarithmic depth-scale). This cell is shifted northward in model R4 as compared to R9. Both KEB parameterizations restore the correct position of the bottom cell at about 30^oN. The upper northern cell acquires correct shape as a result of applying the

KEBs. The northern bottom cell is better reproduced by the stochastic model R4 (see -1.5 isoline in Figure 3).

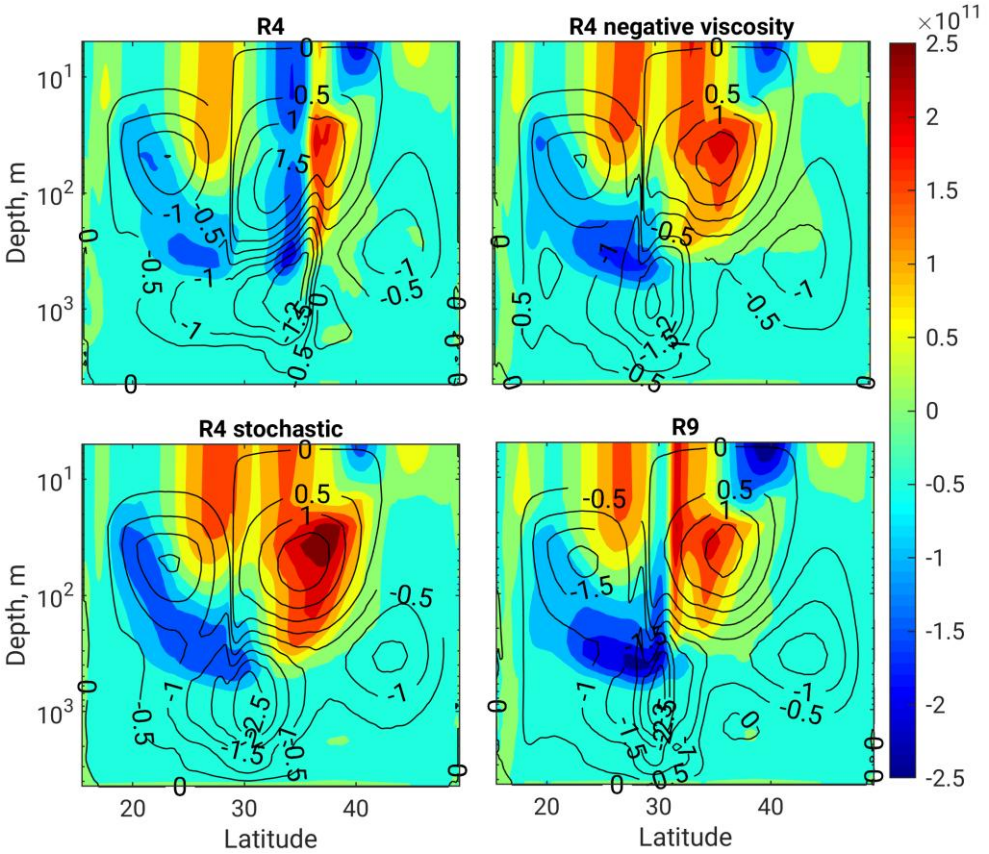

Figure 3. In colour: 20-year mean eddy meridional heat transport integrated zonally, W/m. In contours: 20-year mean meridional overturning streamfunction Ψ_{MOC} in Sverdrups. R4 – eddy-permitting model, R9 – eddy-resolving model, R4 negative viscosity and R4 stochastic – eddy-permitting models with KEB parameterizations.

We study the time variability of the models by computing the time power density of the surface EKE, which is shown in Figure 4. The power density is averaged over a white rectangle shown in Figure 1 to reduce its oscillations and to exclude its strong dependence on the WBC separation point. The spectra consist of two power-law intervals and a long-period tail. The short-period power law ν^{-4} possibly corresponds to the wave motions, while the middle-period ν^{-2} possibly corresponds to the mesoscale turbulence. Both power-law intervals are underestimated in model R4. The KEB parameterizations allow one to increase the power density in the middle-period interval up to the level of model R9. The negative viscosity KEB also improves the power density in the short-period interval. The stochastic KEB gives discrepancy with model R9 in the short-period interval and has a singularity near 1-day oscillation. We decided that the white-noise parameterization excites inertial waves which have a similar period. Earlier it was not reported anywhere that KEB with the white-noise stochastic process excites inertial waves, possibly since most works consider quasi-geostrophic equations (as [8] and [10]), where inertial oscillations are filtered out. We have tried a simple modification of the stochastic KEB, including a temporal correlation with a lag of 10 days to force only the middle-period interval. Correlated noise was generated using an autoregressive model of order 1 (AR-1), as [7] suggests. The time-correlated stochastic KEB does not excite inertial oscillations (not shown), but it

has one moderate drawback: there is no more exact formula for the energy generation like (15), and it introduces one free parameter to be tuned by hand.

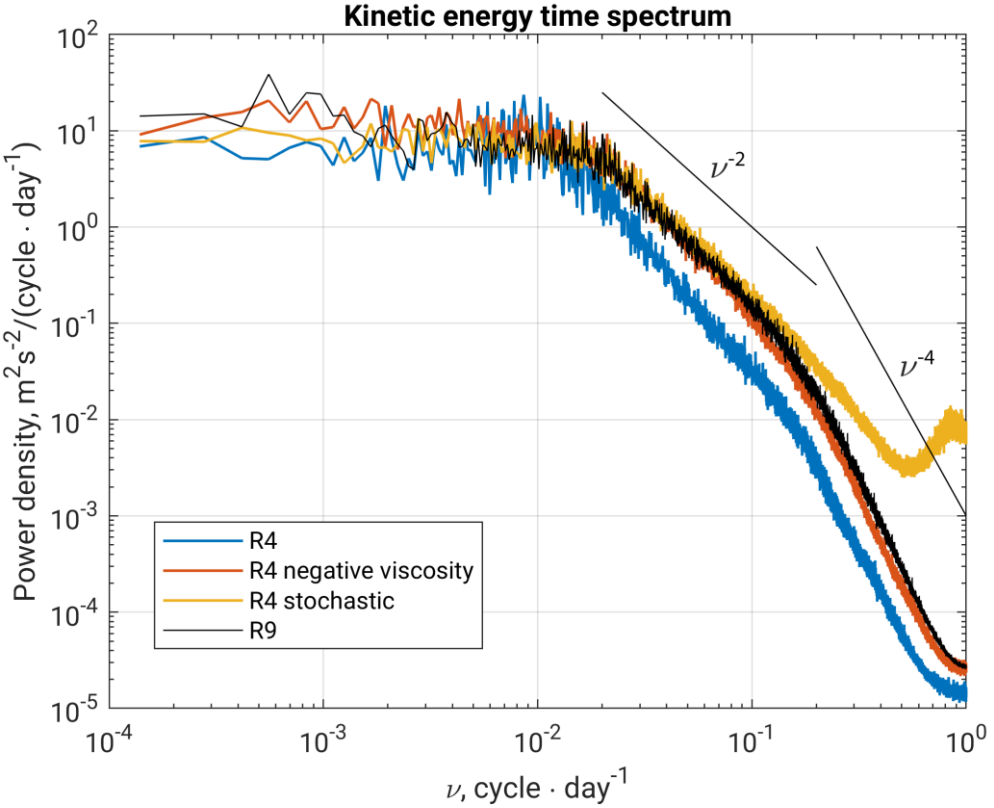

Figure 4. Time power density of surface EKE. Density is averaged over a white rectangle shown in Figure 1. R4 – eddy-permitting model, R9 – eddy-resolving model, R4 negative viscosity and R4 stochastic – eddy-permitting models with KEB parameterizations. Time series correspond to the last 20 years.

Finally, let us consider snapshots of relative vorticity (see Figure 1). The R4 and R9 solutions are highly different in the number of turbulent eddies and filaments. Both KEB parameterizations induce eddy activity in model R4, but in different way. The stochastic KEB solution looks like "synthetic" turbulence which consists of turbulent eddies without filaments and it similar in the shape of its eddies to the stochastic KEB tendency itself. The amount of undesirable noise in the solution can be reduced if the time-correlated stochastic process is used (not shown). The negative viscosity KEB, on the contrary, amplifies the existing filaments and large eddies, but the solution suffers from the absence of small-scale features.

5. Conclusions

In this work, we have demonstrated that simple kinetic energy backscatter (KEB) parameterizations accounting for a badly resolved barotropic inverse energy cascade are able to improve general ocean circulation models with an eddy-permitting resolution. The novelty of this work is the use and comparison of the two KEBs for the primitive equations of the ocean. Both KEBs give similar improvements in the mean characteristics. Specifically, the mesoscale eddies are amplified and, consequently, eddy kinetic energy (EKE) rises. As a result, the eddy meridional heat transport near the surface and in a moderately deep ocean was restored. Large errors in sea surface temperature and height were reduced in the region of jet separation. Also, the bottom cell of the meridional overturning circulation (MOC) was shifted southward, as in the high resolution model. A moderate difference concerns the bottom northern MOC cell, which is better reproduced with the stochastic KEB. It has

been shown that the KEBs effectively improve the time power spectra of EKE, but a white-noise process can lead to an undesirable generation of inertial waves, which can be overcome by introducing a time-correlated stochastic process. The major difference between the KEBs is in the solution type. The stochastic KEB seems to introduce too much small eddies without filaments, but the negative viscosity one amplifies the existing filament-eddy field. It is possible that they can be effectively used together. Future work will be devoted to studying more realistic ocean configurations with varying ocean depth and spherical geometry.

Acknowledgments
The work was supported by the Russian Science Foundation (grant 17-17-01210, development of subgrid turbulence models) and the Russian Foundation for Basic Research (grant 18-05-60184, calculations with idealized ocean model and analysis of results).

References
[1] Haarsma R *et al* 2016 *Geosci. Model Dev.* **9** 4185-4208
[2] Gent P and McWilliams J 1990 *J. of Phys. Oceanography* **20** 150-55
[3] Madec J *et al* 1997 Ocean general circulation model reference manual. *Note du Pôle de modélisation*
[4] Bernard B *et al* 2006 *Ocean dynamics* **56** 543-67
[5] Kraichnan R 1967 *The Phys. of Fluids* **10** 1417-23
[6] Frederiksen J and Davies A 1997 *J. of the Atmos. Sci.* **54** 2475-92
[7] Berner J, Shutts G, Leutbecher M and Palmer T 2009 *J. of the Atmos. Sci.* **66** 603-26
[8] Jansen M and Held I 2014 *Ocean Modelling* **80** 36-48
[9] Jansen M, Held I, Adcroft A and Hallberg R 2015 *Ocean Modelling* **94** 15-26
[10] Grooms I, Lee Y and Majda A 2015 *Multiscale Model.&Sim.* **13** 1001-21
[11] Perezhogin P, Glazunov A and Gritsun A 2019 *Rus. J. of Num. Anal. and Math. Model.* **34**(4) 197-213
[12] Juricke S, Danilov S, Kutsenko A and Oliver M 2019 *Ocean Model.* **138** 51-67
[13] Levy M *et al* 2010 *Ocean Model.* **34** 1-15
[14] Madec G *et al* 2015 NEMO ocean engine
[15] Kraichnan R 1976 *J. of Atm. Sci.* **33** 1521-36
[16] Zurita-Gotor P, Held I and Jansen M 2015 *J. of Adv. In Modeling Earth Sys.* **7** 1117-35
[17] Eden C and Greatbatch R 2008 *Ocean Modelling* **20** 223-39
[18] Carati D, Ghosal S and Moin P 1995 *Phys. Of Fluids* **7** 606-16
[19] Alvelius K 1999 *Phys. Of Fluids* **11** 1880-89